IEEE Access
Multidisciplinary | Rapid Review | Open Access Journal

Received November 17, 2020, accepted November 22, 2020, date of publication November 27, 2020,
date of current version December 10, 2020.

Digital Object Identifier 10.1109/ACCESS.2020.3041192

Received-Signal-Strength (RSS) Based 3D Visible-Light-Positioning (VLP) System Using Kernel Ridge Regression Machine Learning Algorithm With Sigmoid Function Data Preprocessing Method

YU-CHUN WU[1], CHI-WAI CHOW[1], (Senior Member, IEEE), YANG LIU[2], YUN-SHEN LIN[1], CHONG-YOU HONG[1], DONG-CHANG LIN[1], (Graduate Student Member, IEEE), SHAO-HUA SONG[1], AND CHIEN-HUNG YEH[3], (Member, IEEE)

[1]Department of Photonics, College of Electrical and Computer Engineering, National Chiao Tung University, Hsinchu 30010, Taiwan
[2]Philips Electronics Ltd., Shatin, Hong Kong
[3]Department of Photonics, Feng Chia University, Taichung 40724, Taiwan

Corresponding authors: Chi-Wai Chow (cwchow@faculty.nctu.edu.tw) and Chien-Hung Yeh (yeh1974@gmail.com)

This work was supported by the Ministry of Science and Technology, Taiwan, R.O.C., under Grant MOST-109-2221-E-009-155-MY3 and Grant MOST-107-2221-E-009-118-MY3.

ABSTRACT In this work, we propose and demonstrate a received-signal-strength (RSS) based visible-light-positioning (VLP) system using sigmoid function data preprocessing (SFDP) method; and apply it to two types of regression based machine learning algorithms; including the second-order linear regression machine learning (LRML) algorithm, and the kernel ridge regression machine learning (KRRML) algorithm. Experimental results indicate that the use of SFDP method can significantly improve the positioning accuracies in both the LRML and KRRML algorithms. Besides, the SFDP with KRRML scheme outperforms the other three schemes in terms of position accuracy, with the experimental average positioning error of about 2 cm in both horizontal and vertical directions.

INDEX TERMS Visible light communication (VLC), visible light positioning (VLP), light-emitting-diode (LED), machine learning.

I. INTRODUCTION

Due to the growing popularity of Internet-of-Thing (IoT), smart mobile devices and artificial intelligence (AI), the demand for highly precise indoor positioning is increasing rapidly. Although the Global Positioning System (GPS) is common nowadays, it is not suitable for indoor positioning since the GPS signals sent from the satellites and mobile-phone base stations will be blocked by building walls. Besides GPS, systems such as Bluetooth, Radio Frequency Identification (RFID), Wireless-Fidelity (Wi-Fi), Ultra-Wide Band (UWB), etc. can also provide indoor positioning [1], [2]. For example, the UWB technology is based on transmitting radio-frequency (RF) short pulses with a low duty cycle. This allows accurate localization and tracking of mobile devices in indoor environments [2]. However, these RF based systems could suffer from interferences generated by other RF wireless devices and may not be applicable in RF restricted areas. Visible light communication (VLC) is considered as a promising wireless technology for the future wireless and mobile networks [3]–[9]. It is license-free and electromagnetic interference (EMI) free. It can use the existing light-emitting-diode (LED) lighting infrastructure as transmitter (Tx) to provide illuminance and communication simultaneously. In addition, it can release the pressure on the highly congested RF communication spectrum.

One important feature of VLC is that it can provide efficient indoor visible light positioning (VLP) [10]. Different VLP systems have been proposed. Hybrid VLP/RF systems using ZigBee or RF wireless network

The associate editor coordinating the review of this manuscript and approving it for publication was San-Liang Lee.

were proposed [11], [12]. Besides, VLP using proximity schemes were proposed [13]–[18]. In these schemes, optical-beacon or identifier (ID) emitted by the lamps are used for positioning. Proximity based VLP system using 6-axes sensors (geomagnetic sensor and gravity acceleration sensor) with root-mean-square (RMS) error distribution between 0.3 m to 0.5 m was reported [16]. Besides, proximity based VLP schemes employing classify problem based machine learning model [17] or geometric features of LED image were proposed [18]. VLP using fingerprinting schemes were proposed [19]–[23]. In these systems, the received signals were compared with the existing data-bases for positioning. For examples, these VLP systems required fingerprints, such as correlation sum ratios (CSR) [20], power spectral densities [22], or extinction ratios (ER) [23]. Relatively large data-bases were needed. VLP systems using time-of-arrival (TOA) schemes and time-difference-of-arrival (TDOA) schemes were demonstrated [24]–[26]; however, these schemes required high precision Tx-receiver (Rx) synchronization; and these may complicate the systems. VLP using angle-of-arrival (AOA) schemes [27]–[29] were also reported.

Among these VLP schemes, VLP systems based on received-signal-strength (RSS) have also received much attention [30]–[44]. In these RSS based VLP systems, the received optical power depended on the distance between Tx and Rx. By analyzing the received signal amplitudes or powers from several LEDs, the location information can be obtained. Several RSS-based VLP systems have been summarized in Table 1. The RSS based VLP systems can be implemented by using least square, orthogonal frequency division multiple access (OFDMA), or code division multiple access (CDMA) [30]–[34]. A 3D RSS based VLP system based on trilateration combined with a nonlinear least squares (NLLS) was reported numerically [35] and experimentally [36]. The results show at least 4 light sources arranged not on one circle are required to unambiguously extract the 3D location. A particle-assisted stochastic search (PASS) algorithm was proposed to solve the non-convex optimization problem due to the nonlinear RSS VLC model [37].

Recently many of these RSS based VLP systems employed neural networks, such as two-layer fusion network (TLFN), artificial neural network (ANN), Bayesian regularization deep neural network (BR-DNN), etc [38]–[43] for positioning. Thanks to the high degree of freedom provided by these neural networks, these VLP systems can usually have better positioning accuracies. However, the back-propagation algorithm and iteration method used to train the neural networks may significantly increase the computational complexity. Besides, the learning rate would be difficult to adjust.

In this work proposed here, we propose and experimental demonstrate using simpler regression based machine learning algorithm. In the early VLP studies [44], the positioning error can be reduced from 10 cm to 4 cm when applying machine learning. Because of the noises from the LED transmitters and receiver, slightly different light emission patterns from different LEDs, as well as the LED non-ideal Lambertian light distribution, the RSS positioning based on theoretical model may introduce relatively high positioning uncertainty. Machine learning can provide an adaptive model by taking into account the Tx and Rx noises, and different light emission patterns from LEDs; hence, the positioning accuracy can be enhanced.

In this work, we propose and demonstrate a RSS based VLP system using sigmoid function data preprocessing (SFDP) method; and apply it to two types of regression based machine learning algorithms. The contributions of this article are summarized:

- First, we employ a second-order linear regression machine learning (LRML) algorithm for the 3D positioning system. When comparing the positioning accuracy of the proposed LRML scheme with the traditional RSS scheme by analyzing the received power differences among the Txs [31], it can be observed

TABLE 1. Several recently proposed RSS based VLP systems.

Ref.	Method	2D/ 3D	Coverage	Accuracy	Notes
30	RSS/ Least Square	2D	60×52 cm^2	2.4 cm	Exp't
31	RSS/ Least Square	2D	80×69 cm^2	10cm	Exp't
32	RSS/ Least Square	2D	6×6 m^2	11.2cm	Sim.
33	RSS/ OFDMA	2D	20×20 cm^2	1.68 cm	Exp't
34	RSS/ CDMA	3D	3×3×4 m^3	7.06cm (vertical.); 3.18cm (horizontal.)	Exp't
35	RSS/ Trilateration + NLLS	3D	5×5×5 m^3	5.8 cm	Sim.
36	RSS/ Trilateration + NLLS	3D	4×4×5 m^3	12.7 cm	Exp't
37	RSS/ PASS	3D	9×9×4 m^3	10 cm	Sim.
38	RSS/ TLFN	2D	0.7×0.7× 1.48 m^3	5cm	Exp't
39	RSS/ ANN	3D	4×4×2.5 m^3	12cm	Sim.
40	RSS/BR-DNN	2D	1.8×1.8 m^2	3.4cm	Exp't
41	RSS/ DNN	3D	1.2×1.2× 2 m^3	11.93cm	Exp't
42	RSS/ SVM	2D	5×5 m^2	8.6cm	Sim.
43	RSS/ ANN	3D	0.9×1× 0.4 m^3	0.9cm	Exp't
44	RSS/ LRML	2D	50×50 cm^2	4cm	Exp't
This work	RSS/KRRML	3D	1/2×50×50 ×150 cm^3	2.16cm (vertical.); 1.96cm (horizontal.)	Exp't

that machine learning can enhanced the positioning accuracy by providing models to adapt to different indoor conditions.

- Then, we propose and apply the pre-processing scheme, known as SFDP to the LRML algorithm. It can mitigate the effect of outliers due to the power saturation conditions.
- Besides, we also propose and demonstrate the kernel ridge regression machine learning (KRRML) algorithm for VLP system. The addition of the penalty term in the error function can restrict the weights; hence a more stable model can be obtained in the presence of noises.
- Finally, the proposed SFDF is employed together with the KRRML algorithm. It can be observed that this combined scheme can achieve the highest positioning accuracy.

To sum up, there are 4 schemes in comparison: LRML, SFDP + LRML, KRRML, SFDP + KRRML. Experimental results indicate that the use of SFDP method can significantly improve the positioning accuracies in both the LRML and KRRML models. Besides, the SFDP with KRRML scheme outperforms the other three schemes in terms of position accuracy. The data preprocessing SFDP can provide the sigmoid function with hyperparameter to adjust the sigmoid function curve. It can mitigate the effect of outliers by limiting the effect of high received powers at the edge, as well as enhancing the effect of low received powers at the center of the unit cell. In this proof-of-concept VLP demonstration, the unit cell has the horizontal coverage of 1/2 $\times$ 50 cm $\times$ 50 cm, and the vertical coverage of 135 cm. This is due to the laboratory limitation.

This article is organized as follows. In Section II, we will first discuss the RSS VLP mechanism and experiment. Besides, we will also discuss the proposed algorithms, including the SFDP preprocessing method, LRML and KRRML. In Section III, we will present the 3D experimental results and discussion of different proposed algorithms. Finally, a conclusion will be provided in Section IV.

II. RSS VLP EXPERIMENT, MECHANISM AND ALGORITHMS

A. EXPERIMENTAL SETUP

The proposed RSS based VLP experiment is shown in Fig. 1(a). Here, three commercially available white-light LEDs are used as Txs. Three unique optical IDs in Manchester-coded format encoded onto three RF carrier frequencies (f_1, f_2, f_3) respectively are used to modulate the white-light LEDs. The whole positioning area will be covered by repeated unit cells. These RF carrier frequencies can be repeated and re-used as shown in Fig. 1(b), while the IDs of the entire positioning area are unique and non-repeating. Because the ID is non-repeating in the whole area, if the Rx is at the boundary of two unit cells, its position can also be located no matter which unit cell is used. Fig. 1(c) shows the photograph of the test-bed. The ground truth is provided by a pegboard with x and y coordinate information. A camera

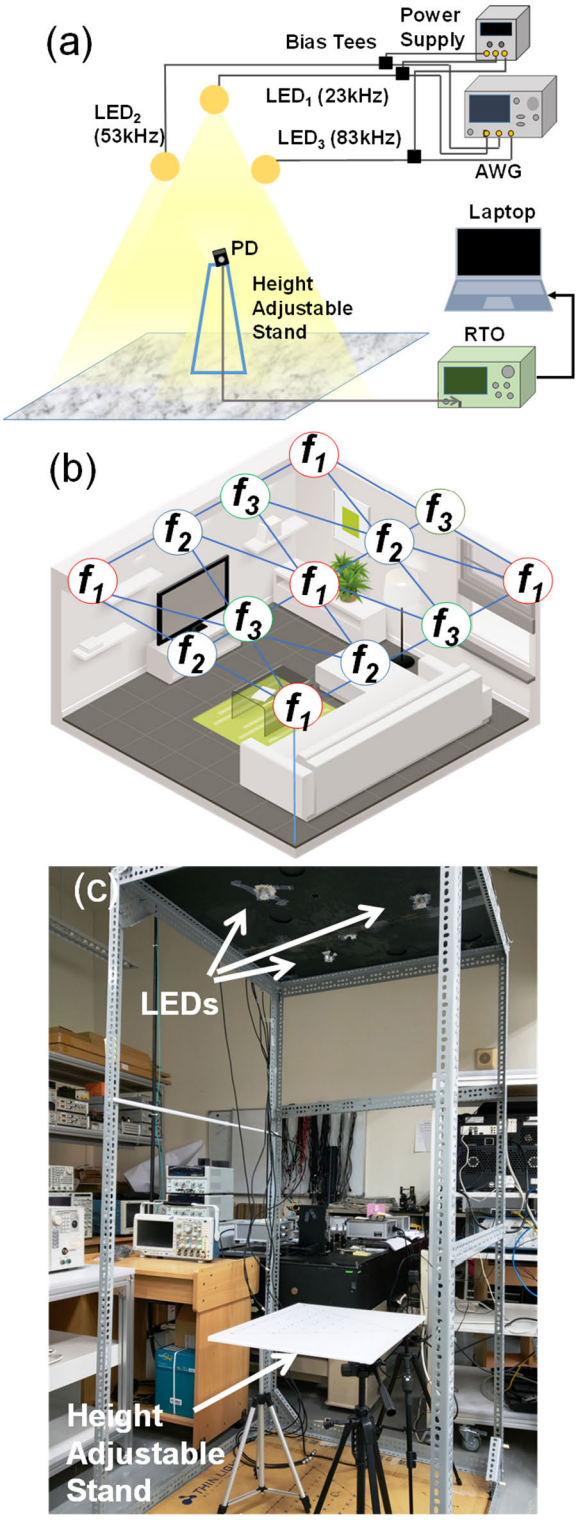

FIGURE 1. (a) Experimental setup of the RSS based VLP system. (b) Proposed VLP scheme using different unit cells to cover the whole indoor areas. AWG: arbitrary waveform generator; RTO: real-time oscilloscope; PD: photo-detector. (c) Photograph of the test-bed.

tripod stands are used to support the pegboard with adjustable z direction.

During positioning, as different LEDs have different IDs, the location of the Rx at which unit cell can be found out at the

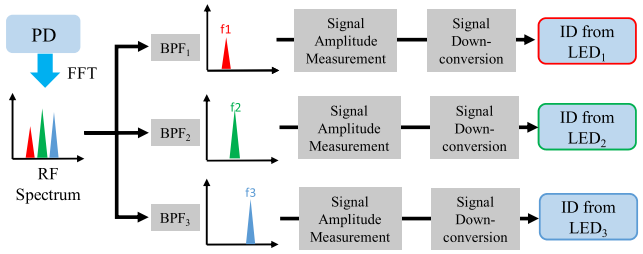

FIGURE 2. Process of retrieving the RSS positioning information and the optical IDs.

beginning. After the identification of the unit cell, the location of the Rx inside that particular unit cell can be found by using RSS. The LED used has a power consumption of 0.5 W using 0.05 A driving current. Its emitting angle is 28°. In the proof-of-concept unit-cell experiment, the RF carrier frequencies are 23 kHz, 53 kHz and 83 kHz respectively. Each RF carrier frequency carriers a Manchester-coded ID at data rate of 6.25 kbit/s. The carrier frequencies used in RSS based positioning should be selected higher than the low cut-off frequency of the bias-tee (> 10 kHz) used, and lower than the modulation speed of the LED (< 1 MHz). Here, we also select the prime numbers in the carrier frequencies so that their harmonic frequencies will not overlap with other carrier frequencies. These signals are generated by an arbitrary wavelength generator (AWG, Tektronix®AFG3252C). The Rx side is a silicon-based photo-detector (PD, Thorlabs®PDA100A2). It consists of a silicon PIN photodiode with a transimpedance amplifier (TIA). The PD is connected to a real-time oscilloscope (RTO, Tektronix®MDO3024) for VLP data retrieval. Ref. [41] defines the unit cell beyond the triangle area provided by the LED lamps. We believe that our proposed schemes can also be applied to a bigger unit cell beyond the triangle area, but may have a larger positioning error.

Fig. 2 shows the mechanism of retrieving the RSS positioning information and the optical IDs. At the Rx, fast Fourier transforms (FFTs) are performed on the received signals to obtain the frequency spectra. After band-pass filtering (BPF), the signal strength of each RF carrier frequency is recorded. Then, each signal is frequency down-converted to obtain the IDs. By decoding the IDs, the unit cell can be located.

B. SIGMOID FUNCTION DATA PREPROCESSING (SFDP) METHOD

In the preprocessing for the LRML and KRRML, the z-score normalization is first applied. The effect of outliers can be mitigated through the z-score normalization. We calculate the z-score of the signals from different LEDs in the training data based on Eq. (1), where q is the strength of each LED, μ is the mean value of all signal strengths from that LED in training data, and σ is the standard deviation in the training data.

$$z(q) = \frac{q - \mu}{\sigma} \tag{1}$$

Usually at the edge or corner of a unit cell, since the Rx is closer to the LED(s), higher signal strength can be detected. On the contrary, the received signal strength is lower at the center of the unit cell. In order to make the trained model suppresses the relative high/low strength values, the data preprocessing SFDP is proposed as shown in Eq. (2),

$$f(z) = \frac{1}{1 + \exp(-bz)} \tag{2}$$

where z is the z-score, and b is a hyperparameter which can adjust the sigmoid function curve. Since the slope of sigmoid function is large when the input is small, and the slope is close to zero when the input is large, it can mitigate the effect of outliers by limiting the effect of high received powers at the edge, as well as enhancing the effect of low received powers at the center of the unit cell. Hence, the positioning accuracy can be enhanced.

C. LINEAR REGRESSION MACHINE LEARNING (LRML) ALGORITHM

The second-order LRML algorithm is expressed in Eq. (3), where $\mathbf{T_p}$ is the predictive coordinate matrix, $\mathbf{W}$ is the weight matrix, $\mathbf{\Phi}$ is the design matrix of RSS, and D is the dimension. Because the proposed VLP system is based on the RSS from three LEDs, the dimension D is equal to 3.

$$\mathbf{T}_p = w^{(0)} + \sum_{i=1}^{D} w^{(i)} q_i + \sum_{i=1}^{D} \sum_{j=1}^{D} w^{(ij)} q_i q_j = \Phi \mathbf{W}_{\mathrm{ML}} \tag{3}$$

The design matrix is expressed in Eq. (4),

$$\mathbf{\Phi} = [\boldsymbol{\phi}(\mathbf{q}_1), \phi(\mathbf{q}_2), \ldots, \phi(\mathbf{q}_N)]^{\mathrm{T}} \tag{4}$$

where N is the number of training data, and $\phi_q(i)$ in Eq. (4) can be expressed as Eq. (5), where q_{n1}, q_{n2} and q_{n3} represent the received signal strengths of 23 kHz, 53 kHz and 83 kHz signals in n_{th} data respectively.

$$\begin{aligned} \phi(\mathbf{q}_n) &= [1, q_{n1}, q_{n2} \cdots, q_{n2} q_{n3}, q_{n3}^2] \\ \mathbf{q}_n &= [q_{n1}, q_{n2}, q_{n3}] \end{aligned} \tag{5}$$

Then, we apply the least squares error function to obtain the weight vector $\mathbf{W_{ML}}$. The error function is expressed as Eq. (6), where $\mathbf{t_n}$ is the target of n_{th} training data.

$$E(\mathbf{W}) = \sum_{n=1}^{N} [\mathbf{t}_n - \mathbf{W}^{\mathrm{T}} \phi(\mathbf{q}_n)]^2 \tag{6}$$

The locations of training data are in x-, y- and z- coordinates. They are put on record during the training process, and they can be represented by the target vector $\mathbf{t}$ as described in Eq. (7).

$$\mathbf{T} = \begin{bmatrix} x_1, x_2, \ldots, x_N \\ y_1, y_2, \ldots, y_N \\ z_1, z_2, \ldots, z_N \end{bmatrix}^{\mathrm{T}} = [\mathbf{t}_1, \mathbf{t}_2, \ldots, \mathbf{t}_N]^{\mathrm{T}} \tag{7}$$

The solution of $\mathbf{W}$ in Eq. (6) can be obtained from Eq. (8).

$$\mathbf{W}_{\mathrm{ML}} = (\mathbf{\Phi}^{\mathrm{T}} \mathbf{\Phi})^{-1} \mathbf{\Phi}^{\mathrm{T}} \mathbf{T} \tag{8}$$

D. KERNEL RIDGE REGRESSION MACHINE LEARNING (KRRML) ALGORITHM

The ridge regression is the least square error function of LRML in Eq. (6) with L2 regularization term scheme [45]. It can be expressed as Eq. (9), where α is the hyperparameter, which controls the relative importance of the regularization term when compared with the sum-of-squares error term. We first discuss the case where the target has only one direction.

$$E(\mathbf{w}) = \sum_{n=1}^{N} [t_n - \mathbf{w}^{\mathrm{T}}\phi(\mathbf{q}_n)]^2 + \frac{\alpha}{2}\mathbf{w}^{\mathrm{T}}\mathbf{w} \tag{9}$$

In order to obtain the optimal $\mathbf{w}$, we set the gradient of E($\mathbf{w}$) with respect to $\mathbf{w}$ equal to zero, and move $\mathbf{w}$ to the left-hand-side of the equal sign. Eq. (10) can be obtained.

$$\begin{aligned}\mathbf{w} &= -\frac{1}{2\alpha}\sum_{n=1}^{N}[\mathbf{w}^{\mathrm{T}}\phi(\mathbf{q}_n) - t_n]\phi(\mathbf{q}_n) \\ &= \sum_{n=1}^{N} a_n\phi(\mathbf{q}_n) = \mathbf{\Phi}^{\mathrm{T}}\mathbf{a}\end{aligned} \tag{10}$$

Here the vector $\mathbf{a} = (a_1, a_2, \ldots, a_N)^{\mathrm{T}}$, and a_n is shown in Eq. (11).

$$a_n = -\frac{1}{\alpha}[\mathbf{w}^{\mathrm{T}}\phi(\mathbf{q}_n) - t_n] \tag{11}$$

We can observe that the solution for $\mathbf{w}$ is in the format of a linear combination of the vectors $\phi_q(n)$. Instead of working with the parameter vector $\mathbf{w}$, we can now reformulate the least squares error function with L2 regularization term Eq. (9) in terms of the parameter vector $\mathbf{a}$, giving rise to a dual representation. After substituting Eq. (10) into Eq. (9), we can obtain the Eq. (12), which is the dual representation of Eq. (9). In the Eq. (12), we define a matrix $\mathbf{K} = \mathbf{\Phi}\mathbf{\Phi}^{\mathrm{T}}$, and the $\mathbf{t}$ is all the coordinate in one direction of data.

$$E(\mathbf{a}) = \frac{1}{2}\mathbf{a}^{\mathrm{T}}\mathbf{K}\mathbf{K}\mathbf{a} - \mathbf{a}^{\mathrm{T}}\mathbf{K}\mathbf{t} + \frac{1}{2}\mathbf{t}^{\mathrm{T}}\mathbf{t} + \frac{\alpha}{2}\mathbf{a}^{\mathrm{T}}\mathbf{K}\mathbf{a} \tag{12}$$

The elements in matrix $\mathbf{K}$ is expressed in Eq. (13), where the kernel function is introduced. In the dual representation in Eq. (12), the error function is based on linear combinations of a kernel function judged at the training data, and makes the solution to the least-squares problem that can be written in terms of the kernel function.

$$K_{nm} = \phi(\mathbf{q}_n)^T\phi(\mathbf{q}_m) = k(\mathbf{q}_n, \mathbf{q}_m) \tag{13}$$

Thus, we can work directly in terms of kernel function and avoid the explicit calculation of the feature vector $\phi(\mathbf{q}_n)$, which allows us implicitly to use feature spaces of dimensionality. In this experiment, the Gaussian radial basis function (GRBF) has been used. The form of GRBF is shown in Eq. (14), in which the γ is a hyperparameter, which can adjust the curve of GRBF.

$$k(\mathbf{q}_n, \mathbf{q}_m) = \exp(-\gamma \|\mathbf{q}_n - \mathbf{q}_m\|^2) \tag{14}$$

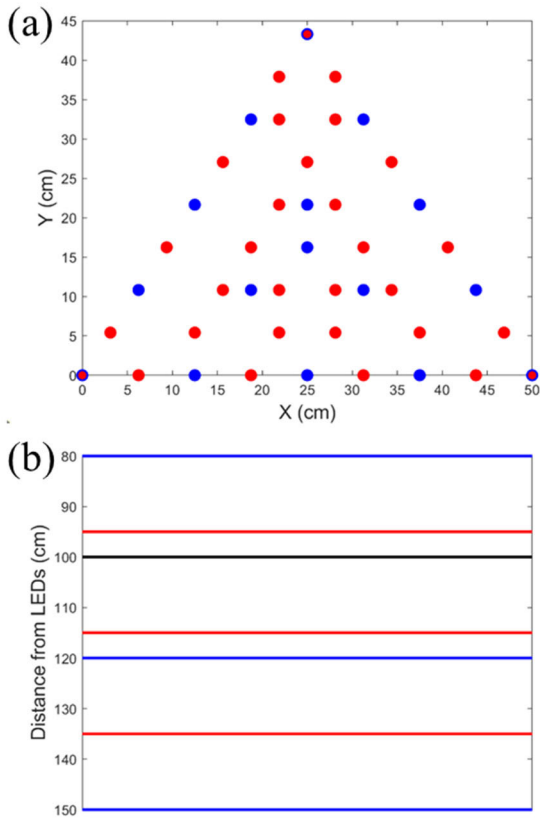

FIGURE 3. (a) Positions of training data (blue) and testing data (red) observed from the top. (b) Positions of the training data plane (blue) and testing data plane (red) observed from the side.

Because the feature vector corresponding to the GRBF has infinite dimensionality, it can adjust relatively easily to fit the strength distribution in the proposed 3D VLP system, and through the regularization term, the model will not be over-fitting. Substituting the result of Eq. (10) into $\mathbf{w}$ in Eq. 11), we can obtain a in Eq. (15).

$$\mathbf{a} = (\mathbf{K} + \alpha\mathbf{I})^{-1}\mathbf{t} \tag{15}$$

We can use the result of Eq. (10) and Eq. (15) to obtain the predictive coordinate as shown in Eq. (16), where $\mathbf{\Phi}_t$ is the design matrix of testing data. The target vector can be expanded into a three-direction matrix. The $\mathbf{\Phi}_t\mathbf{\Phi}^{\mathrm{T}}$ term in Eq. 16) also be calculated in terms of the GRBF in Eq. (14).

$$\mathbf{T}_p = \mathbf{\Phi}_t\mathbf{\Phi}^{\mathrm{T}}(\mathbf{K} + \alpha\mathbf{I})^{-1}\mathbf{T} \tag{16}$$

Fig. 3(a) shows the positions of the training data (blue) and testing data (red) observed from the top of the unit cell. Fig. (b) shows the positions of the training data plane consisting of the training data points (blue) and testing data plane consisting of the testing data points (red) observed from the side of the unit cell. As shown in Fig. 3(b), the training data (blue) are selected at four different vertical distances away from the LED plane: 80 cm, 100 cm, 120 cm, and 150 cm; while the testing data (red) are selected at four different vertical distances away from the LED plane: 95 cm,

TABLE 2. Relations between the methods and the used hyperparameters obtained in experiments.

Method	b	α	γ
LRML			
LRML with SFDP	0.7		
KRRML		0.1	0.1
KRRML with SFDP	0.7	0.3	11

100cm, 115 cm, and 135 cm from the LED plane. As shown in Fig. (a), we select 16 sampling positions as training data in each layer; and we select 30 sampling positions as the testing data in each layer. Each sampling position is measured by 20 times.

Besides, in order to verify the performance of trained model at the training data plane, we also collect the training data and testing data at the same plane at distance of 100 cm (black) away from the LED as shown in Fig. 3(b). It is worth to mention that apart from 3 corner locations at the 100 cm plane, the training data and testing data are not at the same place.

In our defined unit cell shown in Fig. 3, the (x, y, z) coordinates of the LEDs are (0, 0, 0), (25, 43.3, 0) and (50, 0, 0), respectively. All the proposed machine learning algorithms used here are trained using Python®and MATLAB®, and their hyperparameters as shown in Table 2. Amid the 20 training data, 5 of them were randomly selected as the validation data set, and the other 15 were used as the actual training data set. We first use the training data set to train a preliminary model, and then use the validation dataset to find all the hyperparameters used. Only the training data was used to optimize all the hyperparameters through cross-validation and grid search methods [46]. During the training process, the testing data is not used. The training set should be selected uniformly inside the unit cell to achieve better positioning accuracy. In the future work, we will perform experiment with unit cell beyond the area of training data collection. We believe that our proposed algorithms can also be applied to a bigger unit cell beyond the triangle area, but may have larger positioning errors.

III. RESULTS AND DISCUSSION

Fig. 4 shows one example of the measured FFT spectrum measured at one sampling position (25, 16.24, 100). We can observe clearly three signals at carrier frequencies of 23 kHz, 53 kHz and 83 kHz emitted from three white-light LEDs inside a unit cell respectively. Besides, examples of the received IDs down-converted from three RF carrier frequencies are illustrated in Fig. 4(b)-(d).

As discussed in refs. [35], [36], 3D positioning may produce uncertain result when using 3 LEDs and when the vertical height is $<$ 150 cm. When the vertical height is $>$ 150 cm, 4 LEDs are required. The proposed SFDF, LRML and KRRML algorithms can also work well in 4 LEDs or multiple LEDs scenarios.

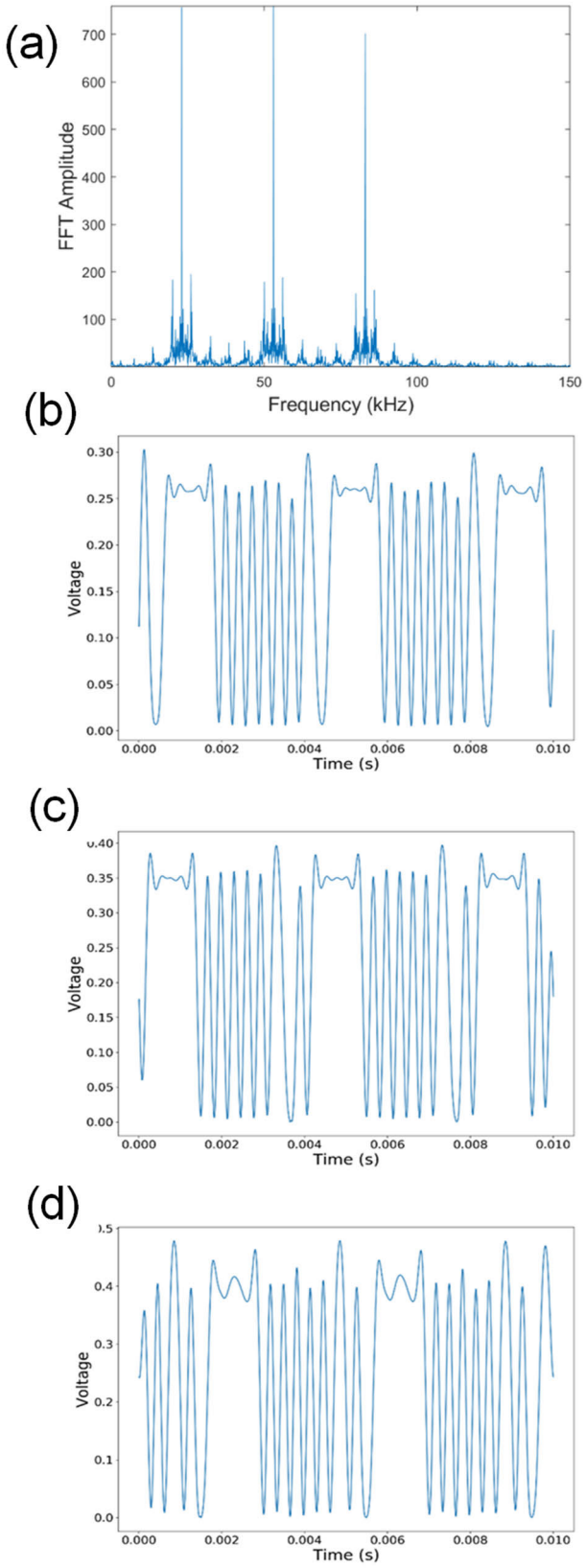

FIGURE 4. One example of (a) the measured FFT spectrum of the received signal at the coordinate of (25, 16.24, 100). (b)-(d) The received IDs down-converted from three RF carrier frequencies.

Figs. 5(a) - (d) show the experimental error distributions of the 3D VLP system using LRML algorithm at vertical distances of 95 cm, 100 cm, 115 cm and 135 cm respectively, away from the LED plane. The radii of the circles shown in Figs. 5(a) - (d) are the experimental average errors in the horizontal direction. The color of the circle is the experimental average error in the vertical direction. It can be clearly observed in Figs. 5(a) - (d) that the average positioning error is relatively large and uneven. High positioning errors are observed at the 135 cm plane away from the LED plane as shown in Fig. 5(d). This is due to the very low signal-to-noise ratio (SNR) received by the PD. The measured illuminance is < 49 lux. Besides, the error distribution is very uneven, particularly in the vertical direction. As shown in Fig. 5(d), we can observe that some positioning errors are > 10 cm (red circle), while some positioning errors are < 2 cm (blue circle).

Then, we introduce the proposed SFDP method to apply the preprocessing step to the LRML algorithm. Figs. 6(a) - (d) show the experimental error distribution of the 3D VLP system using SFDP with LRML algorithm at vertical distances of 95 cm, 100 cm, 115 cm and 135 cm respectively, away from the LED plane. We can observe the improvement in positioning accuracy after the implementation of the SFDP. The average horizontal position error is reduced by 1.04 cm (i.e. improvement of 27.8 %) when the SFDP is applied; and the average vertical position error is reduced by 0.80 cm (i.e. improvement of 22.0 %) when the SFDP is applied. By comparing, for example, the 95 cm and 100 cm planes of Fig. 5 and Fig. 6, it can be observed that the positioning errors, particularly at the edges of unit cell are reduced after the implementation of the proposed SFDP. The data preprocessing SFDP can provide the sigmoid function with hyperparameter to adjust the sigmoid function curve. Since the slope of sigmoid function is large when the input is small, and the slope is close to zero when the input is large, it can mitigate the effect of outliers by limiting the effect of high received powers at the edge, as well as enhancing the effect of low received powers at the center of the unit cell. Hence, the positioning accuracy can be enhanced.

In order to investigate experimentally whether the error is reduced by the sigmoid function, we calculate the coefficient of variation (CV) of the range of the received signal strength change of each LED at each training location, as shown in Table 3. The CV is a standardized measure of dispersion of a distribution, and it is defined as the ratio of the standard deviation to the mean value. As shown in Table 3, after nonlinear conversion through the SFDP, the CVs of the received signal strength are decreased by 16.0%, 20.7%, and 23.2% at the carrier frequencies of 23 kHz, 53 kHz, and 83k Hz LEDs respectively. As aforementioned, SFDP can make the trained model insensitive to changes of signal strength at the edge and the center of unit cell.

Then we apply the KRRML algorithm to further improve the positioning accuracy. Figs. 7(a) - (d) show the experimental error distribution of the 3D VLP system using KRRML algorithm at vertical distances of 95 cm, 100 cm, 115 cm and 135 cm respectively, away from the LED plane. By comparing Fig. 5 and Fig. 7, it can be observed that employing

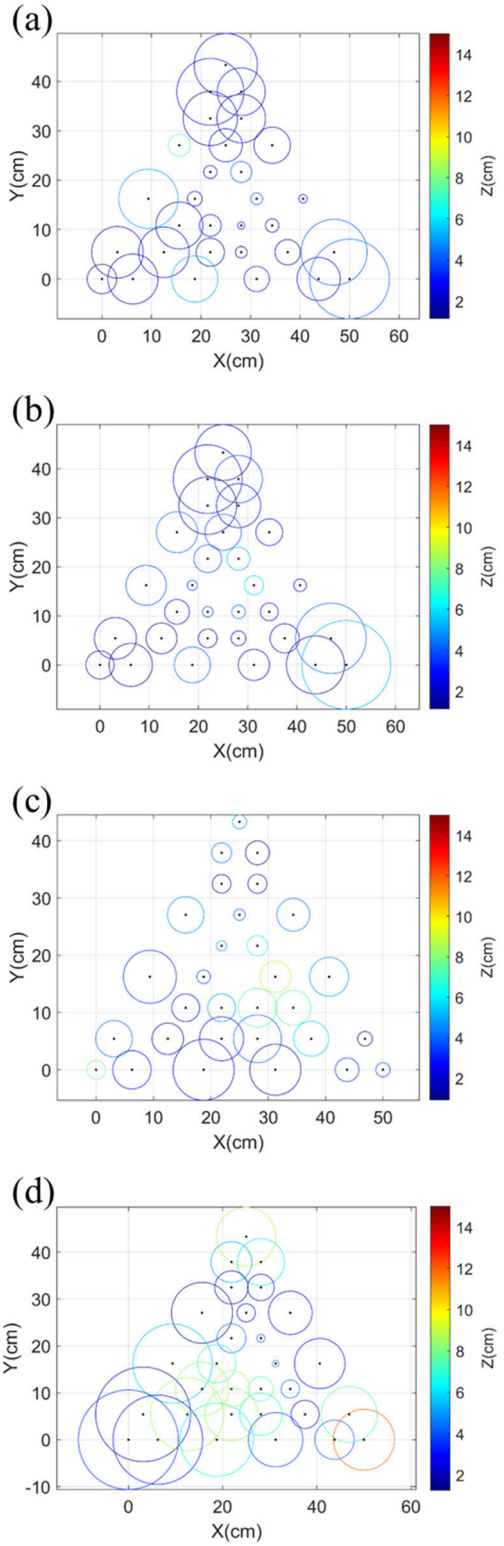

FIGURE 5. Experimental error distribution diagram of the 3D VLP system using LRML at vertical distances of (a) 95 cm, (b) 100 cm, (c) 115 cm and (d) 135 cm away from LED plane.

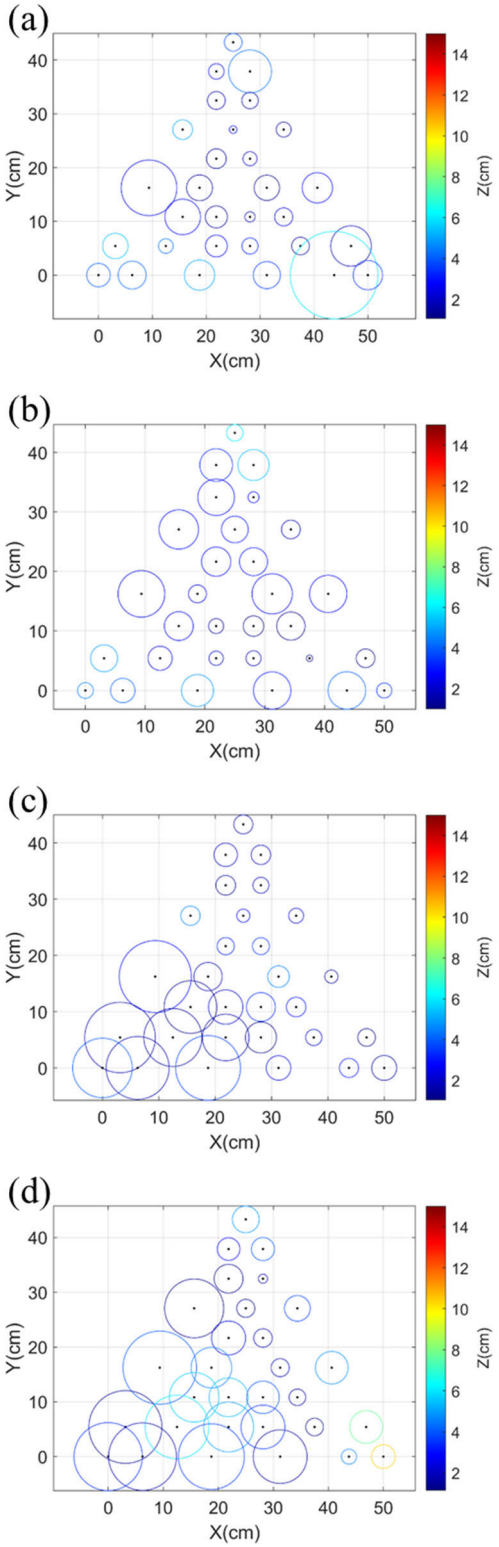

FIGURE 6. Experimental error distribution diagram of the 3D VLP system using LRML and SFDP at vertical distances of (a) 95 cm, (b) 100 cm, (c) 115 cm and (d) 135 cm away from LED plane.

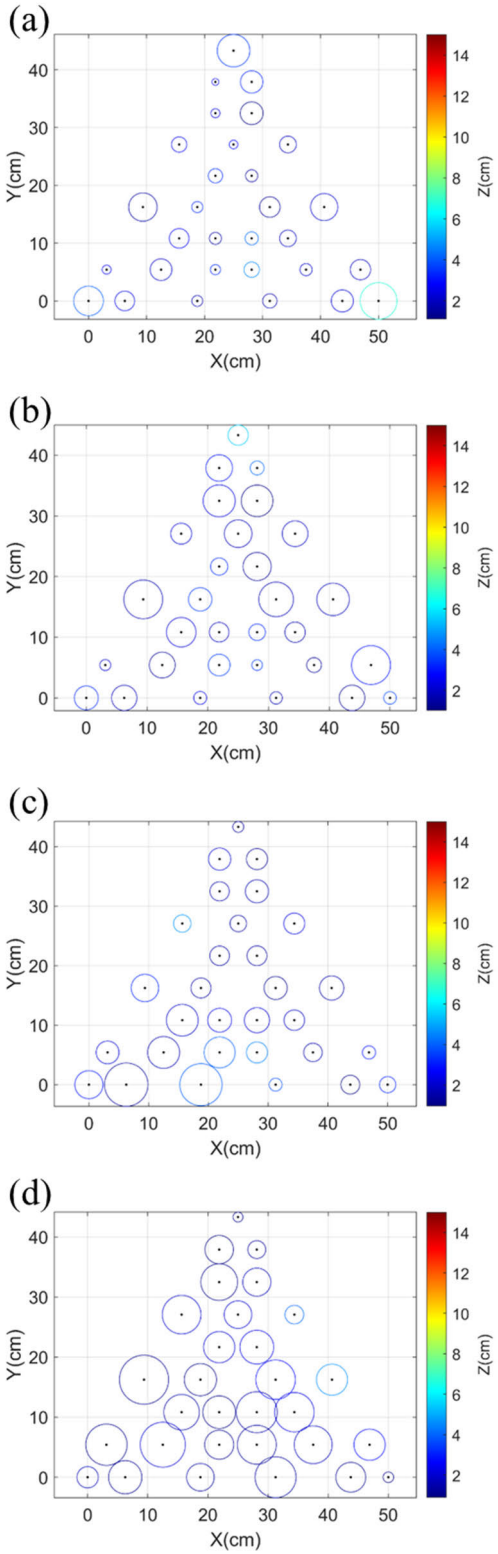

FIGURE 7. Experimental error distribution diagram of the 3D VLP system using KRRML at vertical distances of (a) 95cm, (b) 100 cm, (c) 115 cm and (d) 135 cm away from LED plane.

the KRRML can significantly reduce the positioning error. Besides, the error distribution becomes more uniform. There are still some non-circularly symmetric error-distributions, and these could be due to the hardware issues, such as the slightly different light emission patterns from different LEDs, as well as the LED non-ideal Lambertian light

TABLE 3. The coefficient of variation (CV) of the RSS change range of each LED received at each training location.

LED	CV W/O SFDP	CV W/ SFDP
23 kHz	84.7 %	68.7 %
53 kHz	89.2 %	68.5 %
83 kHz	90.3 %	67.1 %

distribution. By comparing the experimental results of using the LRML algorithm and KRRML algorithm, the average horizontal position error is reduced by 1.74 cm (improvement of 46.5 %); and the average vertical position error is reduced by 1.41 cm (improvement of 38.7 %). As aforementioned, the feature vector corresponding to the GRBF has infinite dimensionality, it can be adjusted relatively easily to fit the strength distribution in the proposed 3D VLP system.

Afterwards, we evaluate the performance of the SFDP with KRRML algorithm. Figs. 8(a) - (d) show the experimental error distribution of the 3D VLP system using KRRML and SFDP algorithm at vertical distances of 95 cm, 100 cm, 115 cm and 135 cm respectively, away from the LED plane. Although the improvement is not significant, we still can achieve reduction in the positioning errors. The average horizontal position error is reduced by 0.04 cm (i.e. improvement of 2.0 %) when the SFDP is applied; and the average vertical position error is reduced by 0.07 cm (i.e. improvement of 3.1 %) when the SFDP is applied. Although the position errors of the KRRML algorithm is quite low, the introduction of the proposed SFDP can still reduced by the positioning errors from 2.0 to 3.1 %.

Table 4 summaries the average horizontal and vertical positioning errors when applying the LRML, LRML with SFDP, KRRML, and KRRML with SFDP. We can observe that when using the LRML with SFDP, the average positioning error in both directions is within 4 cm. When using the KRRML with SFDP, the average positioning error in both directions is about 2 cm. Due to the hardware issues discussed above, the error distribution in the horizontal plane may not directly related to the error distribution in the vertical plane. Both horizontal and vertical positioning errors include both drifting and noises.

In this proof-of-concept VLP demonstration, the unit cell has the horizontal coverage of 1/2 $\times$ 50 cm $\times$ 50 cm, and the vertical coverage of 135 cm. This is due to the laboratory limitation. In the future work, we will perform experiment with unit cell beyond the area of training data collection. We believe that our proposed algorithms can also be applied to a bigger unit cell beyond the triangle area, but may have larger positioning errors. It is also worth to note that during application of SFDP, the Rx cannot be placed too close or too far to either LED. Otherwise, they may be considered as outliers. This could constrain the coverage of the system.

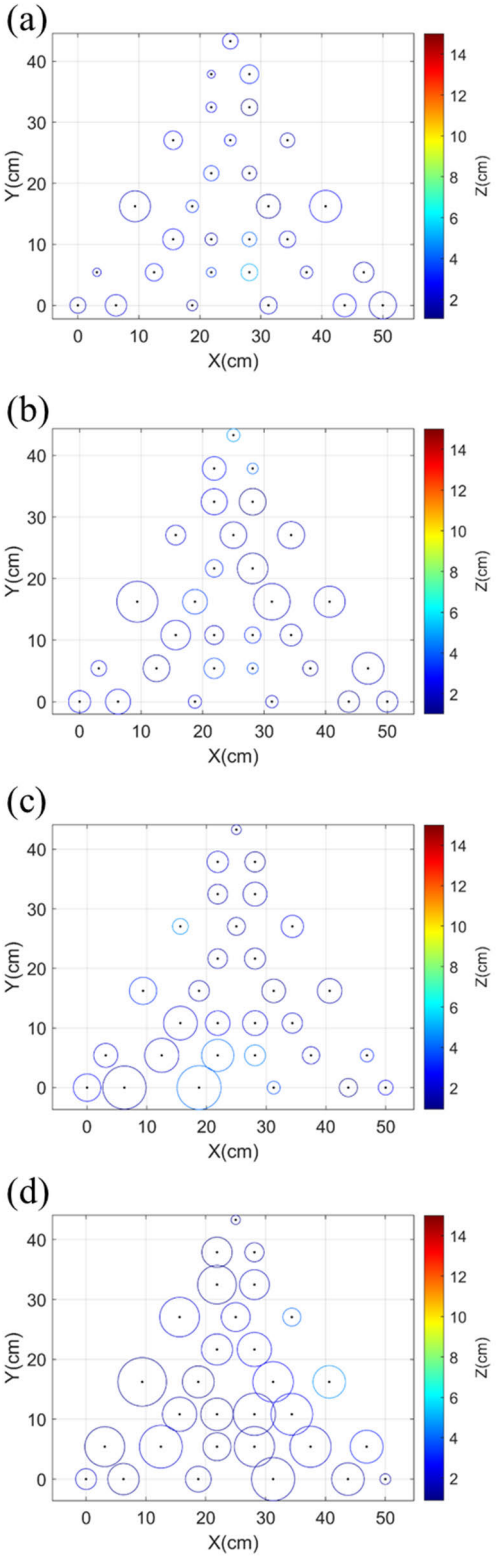

FIGURE 8. Experimental error distribution diagram of the 3D VLP system using KRRML and SFDP at vertical distances of (a) 95cm, (b) 100 cm, (c) 115 cm and (d) 135 cm away from LED plane.

Figs. 9(a) - (d) show the experimental cumulative distribution function (CDF) of the horizontal positioning errors

TABLE 4. The average positioning error of using different machine learning algorithm.

Method	Ave. horizontal error	Ave. vertical error
LRML	3.74 cm	3.64 cm
LRML with SFDP	2.70 cm	2.84 cm
KRRML	2.00 cm	2.23 cm
KRRML with SFDP	1.96 cm	2.16 cm

after applying different machine learning models at vertical distances of 95 cm, 100 cm, 115 cm and 135 cm respectively, away from the LED plane. The experimental CDF curve is obtained by first fixing the integer positioning error in the x-axis (i.e., 1, 2, 3, ... cm); then the cumulative number of data occurrence with errors the fixed integer positioning error is plotted on the y-axis. We can observe the CDF performances of the four schemes; showing that the LRML with SFDP is better than the LRML; and the KRRML with SFDP is better than the KRRML. At the vertical position of 95 cm away from the LED plane as shown in Fig. 9(a), 100 % of the experimental data have positioning error within 3 cm when using the KRRML with SFDP; while 100 % of the data have positioning error within 4 cm when using the KRRML only. Besides, 100 % of the data have positioning error within 9 cm when using the simplest LRML model only. When the vertical position of 135 cm away from the LED plane as shown in Fig. 9(d), 100 % of the experimental data have positioning error within 5 cm when using the KRRML with SFDP; while 100 % of the data have positioning error within 11 cm when using the simplest LRML model only. Besides, the CDFs of both KRRML with SFDP and the KRRML only have nearly the same performances.

Figs. 10(a) - (d) show the experimental CDF of the vertical position error at vertical directions at 95 cm, 100 cm, 115 cm and 135 cm away from LEDs. Similarly, we can clearly observe that the CDF performances of the four schemes; showing that the LRML with SFDP is better than the LRML; and the KRRML with SFDP is better than the KRRML. At the vertical position of 95 cm away from the LED plane as shown in Fig. 10(a), 100 % of the experimental data have positioning error within 6 cm when using the KRRML with SFDP; while 100 % of the data have positioning error within 7 cm when using the KRRML only. Besides, 100 % of the data have positioning error within 8 cm when using the simplest LRML model only. When the vertical position of 135 cm away from the LED plane as shown in Fig. 9(d), 100 % of the experimental data have positioning error within 5 cm when using the KRRML with SFDP; while 100 % of the data have positioning error within 12 cm when using the simplest LRML model only. Similarly to the case of horizontal CDF, the CDFs of both KRRML with SFDP and the KRRML only have nearly the same performances.

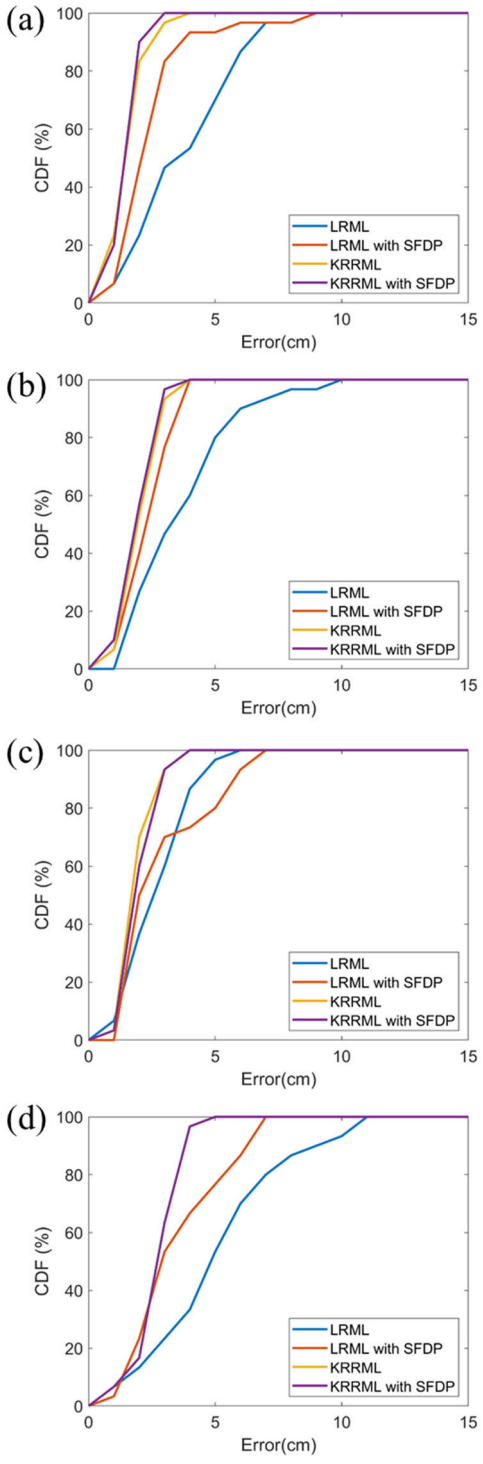

FIGURE 9. The experimental CDF against positioning error in horizontal direction at vertical distances of (a) 95 cm, (b) 100 cm, (c) 115cm and (d) 135 cm away from LEDs.

As discussed in the introduction, VLP can provide many interesting applications, such as providing indoor location and navigation information similar to GPS. Besides, VLP can also be applied for asset tracking in schools, supermarkets, and hospitals.

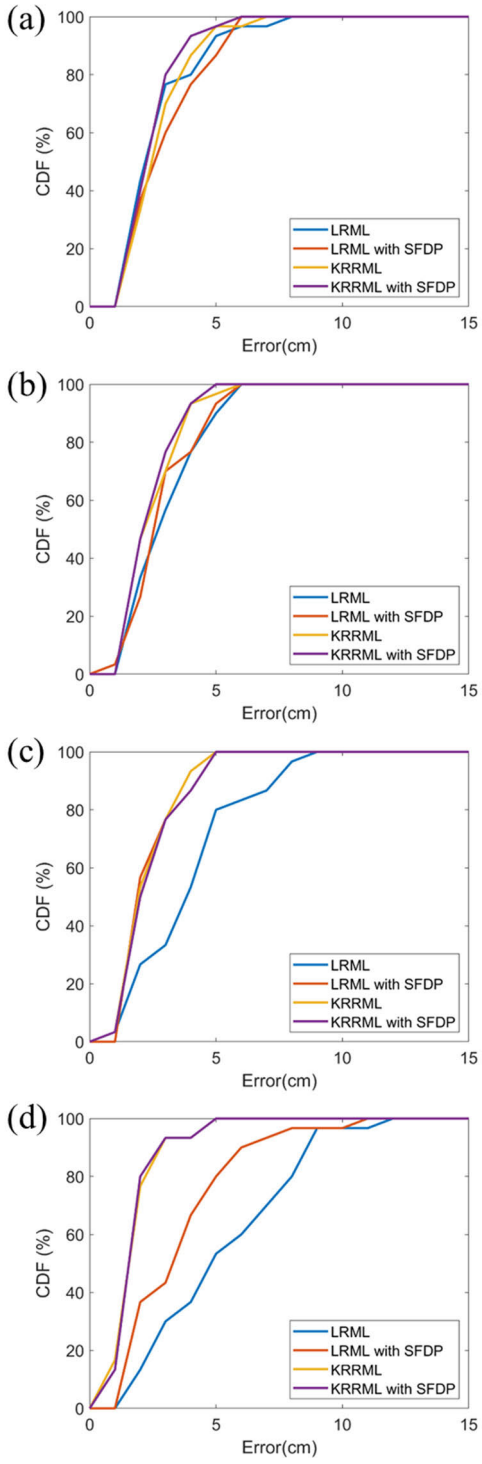

FIGURE 10. The experimental CDF of the vertical position error at vertical direction at (a) 95 cm, (b) 100 cm, (c) 115cm and (d) 135 cm away from LEDs.

IV. CONCLUSION

In this work, we proposed and demonstrated an RSS based VLP system using SFDP method; and applied it to two types of regression based machine learning algorithms; including the second-order LRML algorithm, and the KRRML algorithm. Experimental results indicated that the use of SFDP method can significantly improve the positioning accuracies in both the LRML and KRRML algorithms. Besides, the SFDP with KRRML scheme outperformed the other three schemes in terms of position accuracy. The actual unit cell in this proof-of-concept demonstration had the horizontal coverage of 1/2 (50 cm x 50 cm), and the vertical coverage of 95 cm to 135 cm (i.e. 40 cm). The average horizontal and vertical positioning errors of the KRRML with SFDP algorithms were 1.96 cm and 2.16 cm respectively.

By comparing the LRML model without and with the preprocessing step SFDP, the average horizontal positioning accuracy was improved by 27.8 %; and the average vertical positioning accuracy was improved by 22.0 %. Besides, we also proposed and demonstrated the KRRML model. By comparing the LRML model and KRRML model, the average horizontal positioning accuracy was improved by 46.5 %; and the average vertical positioning accuracy was improved by 38.7 %. Although the positioning errors of the KRRML model is quite low, the introduction of the proposed SFDP can still reduced by the positioning errors from 2.0 to 3.1 %.

REFERENCES

[1] A. Yassin, Y. Nasser, M. Awad, A. Al-Dubai, R. Liu, C. Yuen, R. Raulefs, and E. Aboutanios, "Recent advances in indoor localization: A survey on theoretical approaches and applications," *IEEE Commun. Surveys Tuts.*, vol. 19, no. 2, pp. 1327–1346, 2nd Quart., 2017.

[2] S. Gezici, Z. Tian, G. B. Giannakis, H. Kobayashi, A. F. Molisch, H. V. Poor, and Z. Sahinoglu, "Localization via ultra-wideband radios: A look at positioning aspects for future sensor networks," *IEEE Signal Process. Mag.*, vol. 22, no. 4, pp. 70–84, Jul. 2005.

[3] C. W. Chow, C. H. Yeh, Y. Liu, and Y. F. Liu, "Digital signal processing for light emitting diode based visible light communication," *IEEE Photon. Soc. Newslett.*, vol. 26, no. 5, pp. 9–13, Oct. 2012.

[4] C. H. Yeh, Y. L. Liu, and C. W. Chow, "Real-time white-light phosphor-LED visible light communication (VLC) with compact size," *Opt. Exp.*, vol. 21, pp. 26192–26197, 2013.

[5] C. W. Chow, C. H. Yeh, Y. Liu, Y. Lai, L. Y. Wei, C. W. Hsu, G. H. Chen, X. L. Liao, and K. H. Lin, "Enabling techniques for optical wireless communication systems," in *Proc. OFC*, 2020, Paper M2F.1.

[6] C.-T. Tsai, C.-H. Cheng, H.-C. Kuo, and G.-R. Lin, "Toward high-speed visible laser lighting based optical wireless communications," *Prog. Quantum Electron.*, vol. 67, Sep. 2019, Art. no. 100225.

[7] C.-Y. Li, H.-W. Wu, H.-H. Lu, W.-S. Tsai, S.-E. Tsai, and J.-Y. Xie, "A hybrid Internet/CATV/5G fiber-FSO integrated system with a triple-wavelength polarization multiplexing scenario," *IEEE Access*, vol. 7, pp. 151023–151033, 2019.

[8] C. H. Chang, C. Y. Li, H. H. Lu, C. Y. Lin, J. H. Chen, Z. W. Wan, and C. J. Cheng, "A 100-Gb/s multiple-input multiple-output visible laser light communication system," *J. Lightw. Technol.*, vol. 32, no. 24, pp. 4121–4127, Dec. 15, 2014.

[9] H. Y. Lan, I. C. Tseng, Y. H. Lin, G. R. Lin, D. W. Huang, and C. H. Wu, "High-speed integrated micro-LED array for visible light communication," *Opt. Lett.*, vol. 45, no. 8, pp. 2203–2206, 2020.

[10] J. Armstrong, Y. Sekercioglu, and A. Neild, "Visible light positioning: A roadmap for international standardization," *IEEE Commun. Mag.*, vol. 51, no. 12, pp. 68–73, Dec. 2013.

[11] Y. U. Lee, S. Baang, J. Park, Z. Zhou, and M. Kavehrad, "Hybrid positioning with lighting LEDs and Zigbee multihop wireless network," *Proc. SPIE*, vol. 8282, Jan. 2012, Art. no. 82820L-1.

[12] Y. Lee and M. Kavehrad, "Two hybrid positioning system design techniques with lighting LEDs and ad-hoc wireless network," *IEEE Trans. Consum. Electron.*, vol. 58, no. 4, pp. 1176–1184, Nov. 2012.

[13] S. Ayub, B. Honary, S. Kariyawasam, and M. Honary, "Visible light ID system for indoor localization," in *Proc. ICWMMN*, 2013, pp. 254–257.

[14] M. Nakajima and S. Haruyama, "New indoor navigation system for visually impaired people using visible light communication," *EURASIP J. Wireless Commun. Netw.*, vol. 2013, p. 37, Dec. 2013.
[15] G. del Campo-Jimenez, J. M. Perandones, and F. J. Lopez-Hernandez, "A VLC-based beacon location system for mobile applications," in *Proc. ICL-GNSS*, Turin, Italy, 2013, pp. 1–4.
[16] C. Sertthin, E. Tsuji, M. Nakagawa, S. Kuwano, and K. Watanabe, "A switching estimated receiver position scheme for visible light based indoor positioning system," in *Proc. 4th Int. Symp. Wireless Pervas. Comput.*, Melbourne, VIC, Australia, Feb. 2009, pp. 1–5.
[17] C. Y. Xie, W. P. Guan, Y. X. Wu, L. T. Fang, and Y. Cai, "The LED-ID detection and recognition method based on visible light positioning using proximity method," *IEEE Photon. J.*, vol. 10, no. 2, Apr. 2018, Art. no. 7902116.
[18] R. Zhang, W. Zhong, Q. Kemao, and S. Zhang, "A single LED positioning system based on circle projection," *IEEE Photon. J.*, vol. 9, no. 4, Jul. 2017, Art. no. 7905209.
[19] C. Zhao, H. Zhang, and J. Song, "Fingerprint and visible light communication based indoor positioning method," *Proc. ICAIT*, 2017, pp. 204–209.
[20] S. Y. Jung, S. Hann, S. Park, and C. S. Park, "Optical wireless indoor positioning system using light emitting diode ceiling lights," *Microw. Opt. Technol. Lett.*, vol. 54, no. 7, pp. 1611–1626, 2012.
[21] Y. Liu, C.-W. Hsu, H.-Y. Chen, K. Liang, C.-W. Chow, and C.-H. Yeh, "Visible-light communication multiple-input multiple-output technology for indoor lighting, communication, and positioning," *Opt. Eng.*, vol. 54, no. 12, Dec. 2015, Art. no. 120502.
[22] J. Vongkulbhisal, B. Chantaramolee, Y. Zhao, and W. S. Mohammed, "A fingerprinting-based indoor localization system using intensity modulation of light emitting diodes," *Microw. Opt. Technol. Lett.*, vol. 54, no. 5, pp. 1218–1227, May 2012.
[23] S.-H. Yang, D.-R. Kim, H.-S. Kim, Y.-H. Son, and S.-K. Han, "Indoor positioning system based on visible light using location code," in *Proc. ICCE*, 2012, pp. 360–363.
[24] T. Q. Wang, Y. A. Sekercioglu, A. Neild, and J. Armstrong, "Position accuracy of time-of-arrival based ranging using visible light with application in indoor localization systems," *J. Lightw. Technol.*, vol. 31, no. 20, pp. 3302–3308, Oct. 2013.
[25] P. F. Du, S. Zhang, C. Chen, A. Alphones, and W. D. Zhong, "Demonstration of a low-complexity indoor visible light positioning system using an enhanced TDOA scheme," *IEEE Photon. J.*, vol. 10, no. 4, Aug. 2018, Art. no. 7905110.
[26] J. H. Y. Nah, R. Parthiban, and M. H. Jaward, "Visible light communications localization using TDOA-based coherent heterodyne detection," in *Proc. ICP*, Melaka, Malaysia, 2013, pp. 247–249.
[27] M. H. Bergen, X. Jin, D. Guerrero, H. A. L. F. Chaves, N. V. Fredeen, and J. F. Holzman, "Design and implementation of an optical receiver for angle-of-arrival-based positioning," *J. Lightw. Technol.*, vol. 35, no. 18, pp. 3877–3885, Sep. 15, 2017.
[28] H. Steendam, "A 3-D positioning algorithm for AOA-based VLP with an aperture-based receiver," *IEEE J. Sel. Areas Commun.*, vol. 36, no. 1, pp. 23–33, Jan. 2018.
[29] C. Y. Hong, Y. C. Wu, Y. Liu, C. W. Chow, C. H. Yeh, K. L. Hsu, D. C. Lin, X. L. Liao, K. H. Lin, and Y. Y. Chen, "Angle-of-arrival (AOA) visible light positioning (VLP) system using solar cells with third-order regression and ridge regression algorithms," *IEEE Photon. J.*, vol. 12, no. 3, Jun. 2020, Art. no. 7902605.
[30] H.-S. Kim, D.-R. Kim, S.-H. Yang, Y.-H. Son, and S.-K. Han, "An indoor visible light communication positioning system using a RF carrier allocation technique," *J. Lightw. Technol.*, vol. 31, no. 1, pp. 134–144, Jan. 1, 2013.
[31] C. W. Hsu, J. T. Wu, H. Y. Wang, C. W. Chow, C. H. Lee, M. T. Chu, and C. H. Yeh, "Visible light positioning and lighting based on identity positioning and RF carrier allocation technique using a solar cell receiver," *IEEE Photon. J.*, vol. 8, no. 4, Aug. 2016, Art. no. 7905507.
[32] W. Zhang, M. I. S. Chowdhury, and M. Kavehrad, "Asynchronous indoor positioning system based on visible light communications," *Opt. Eng.*, vol. 53, no. 4, Apr. 2014, Art. no. 045105.
[33] B. Lin, X. Tang, Z. Ghassemlooy, C. Lin, and Y. Li, "Experimental demonstration of an indoor VLC positioning system based on OFDMA," *IEEE Photon. J.*, vol. 9, no. 2, Apr. 2017, Art. no. 7902209.
[34] W. Guan, Y. Wu, S. Wen, H. Chen, C. Yang, Y. Chen, and Z. Zhang, "A novel three-dimensional indoor positioning algorithm design based on visible light communication," *Opt. Commun.*, vol. 392, pp. 282–293, Jun. 2017.
[35] D. Plets, Y. Almadani, S. Bastiaens, M. Ijaz, L. Martens, and W. Joseph, "Efficient 3D trilateration algorithm for visible light positioning," *J. Opt.*, vol. 21, no. 5, May 2019, Art. no. 05LT01.
[36] D. Plets, S. Bastiaens, M. Ijaz, Y. Almadani, L. Martens, W. Raes, N. Stevens, and W. Joseph, "Three-dimensional visible light positioning: An experimental assessment of the importance of the LEDs' locations," in *Proc. IPIN*, Pisa, Italy, 2019, pp. 1–6.
[37] B. Zhou, V. Lau, Q. Chen, and Y. Cao, "Simultaneous positioning and orientating for visible light communications: Algorithm design and performance analysis," *IEEE Trans. Veh. Technol.*, vol. 67, no. 12, pp. 11790–11804, Dec. 2018.
[38] X. Guo, F. Hu, N. R. Elikplim, and L. Li, "Indoor localization using visible light via two-layer fusion network," *IEEE Access*, vol. 7, pp. 16421–16430, 2019.
[39] S. Zhang, P. Du, C. Chen, W.-D. Zhong, and A. Alphones, "Robust 3D indoor VLP system based on ANN using hybrid RSS/PDOA," *IEEE Access*, vol. 7, pp. 47769–47780, 2019.
[40] H. Zhang, J. Cui, L. Feng, A. Yang, H. Lv, B. Lin, and H. Huang, "High-precision indoor visible light positioning using deep neural network based on the Bayesian regularization with sparse training point," *IEEE Photon. J.*, vol. 11, no. 3, Apr. 2019, Art. no. 7903310.
[41] P. Du, S. Zhang, C. Chen, H. Yang, W.-D. Zhong, R. Zhang, A. Alphones, and Y. Yang, "Experimental demonstration of 3D visible light positioning using received signal strength with low-complexity trilateration assisted by deep learning technique," *IEEE Access*, vol. 7, pp. 93986–93997, 2019.
[42] H. Tran and C. Ha, "Improved visible light-based indoor positioning system using machine learning classification and regression," *Appl. Sci.*, vol. 9, no. 6, p. 1048, Mar. 2019.
[43] J. He, C. W. Hsu, Q. Zhou, M. Tang, S. Fu, D. Liu, L. Deng, and G. K. Chang, "Demonstration of high precision 3D indoor positioning system based on two-layer ANN machine learning technique," in *Proc. OFC*, 2019, Paper Th3I2.
[44] Y. C. Chuang, Z. Q. Li, C. W. Hsu, Y. Liu, and C. W. Chow, "Visible light communication and positioning using positioning cells and machine learning algorithms," *Opt. Exp.*, vol. 27, pp. 16377–16383, 2019.
[45] C. M. Bishop, *Pattern Recognition and Machine Learning*. New York, NY, USA: Springer, 2006.
[46] S. Raschka and V. Mirjalili, *Python Machine Learning: Machine Learning and Deep Learning with Python, Scikit-Learn, and TensorFlow*. Birmingham, U.K.: Packt Publishing, 2017.

YU-CHUN WU received the master's degree from the Department of Photonics, National Chiao Tung University, Taiwan, in 2020. His research interests include visible light positioning, machine learning, and visible light communication.

CHI-WAI CHOW (Senior Member, IEEE) received the B.Eng. (Hons.) and Ph.D. degrees from the Department of Electronic Engineering, The Chinese University of Hong Kong (CUHK), in 2001 and 2004, respectively. His Ph.D. thesis was on optical label controlled packet switched networks. He was appointed as a Postdoctoral Fellow with CUHK, where he was involved in hybrid integration of photonic components and silicon waveguides. From 2005 to 2007, he was a Postdoctoral Research Scientist with the Department of Physics, Tyndall National Institute, University College Cork, Ireland, where he was involved mainly in two European Union projects—photonic integrated extended metro and access network and transparent ring interconnection using multi-wavelength photonic switches. In 2007, he joined as an Assistant Professor with the Department of Photonics, National Chiao Tung University, Taiwan, where he is currently a Professor. He has also served in many international conferences, including serving as the TPC of ECOC 2020, CLEO-PR 2020, OFC 2021, and ECOC 2021, a Workshop Co-Organizer of the IEEE GLOBECOM 2020, and the Track Chair of OECC 2020.

YANG LIU received the bachelor's degree from the Department of Electronics Engineering, Northwest University, in 2001, the master's degree from the College of Precision Instrument and Opto-electronics Engineering, Tianjin University, in 2004, and the Ph.D. degree from the Department of Electronic Engineering, The Chinese University of Hong Kong (CUHK), in 2007. Her Ph.D. thesis was on silicon photonics and nonlinear effects of silicon waveguides. After graduation, she was appointed as a Post-Doctoral Fellow with the CUHK. In 2007, she was a Visiting Researcher with the Tyndall National Institute, University College Cork, Ireland. Her research interests are silicon photonics, optical nonlinear effects, visible light communications, and optical wireless communications.

YUN-SHEN LIN received the B.S. degree in electronic engineering from National Chiao Tung University, Taiwan. He is currently pursuing the master's degree with the Department of Photonics, National Chiao Tung University, Taiwan. His research interests include visible light communication, optical camera communication, and optical wireless communication.

CHONG-YOU HONG received the B.S. degree from the Department of Photonics, Feng Chia University, Taiwan, in 2018, and the master's degree from the Department of Photonics, National Chiao Tung University, Taiwan, in 2020. His research interests include optical communication and visible light positioning systems.

DONG-CHANG LIN (Graduate Student Member, IEEE) received the bachelor's degree from the Department of Physics, National Central University, in 2019. He is currently pursuing the master's degree with the Department of Photonics, National Chiao Tung University, Taiwan. His research interest includes application of machine learning on visible light communication and positioning.

SHAO-HUA SONG received the B.S. degree with the Department of Photonics, National Cheng Kung University. He is currently pursuing the master's degree with the Department of Photonics, National Chiao Tung University. His research interests include visible light communication, illumination simulation, and machine learning for visible light positioning.

CHIEN-HUNG YEH (Member, IEEE) received the Ph.D. degree from the Institute of Electro-Optical Engineering, National Chiao Tung University, Taiwan, in 2004. In 2004, he joined the Information and Communications Research Laboratories, Industrial Technology Research Institute (ITRI), Taiwan, as a Researcher, where he was promoted to a Principal Researcher for leading the ITRI Industrial-Academic Projects in 2008. In 2014, he joined the Faculty of Department of Photonics, Feng Chia University, Taiwan, where he is currently a Professor. His research interests include optical fiber communication, fiber laser and amplifier, optical PON access, MMW communication, fiber sensor, and Li-Fi-based technologies.